Batteries & Supercaps

Research Article
doi.org/10.1002/batt.202300183

Chemistry Europe
European Chemical Societies Publishing

www.batteries-supercaps.org

Polysiloxane/Poly(vinylidene fluoride)-co-Hexafluoropropylene Polymer Blend-based Lithium-Ion Conducting Polymer Electrolytes for Room-Temperature Lithium-Metal Batteries

Asuman Celik-Kucuk*[a] and Takeshi Abe[a]

To harness the synergistic effect of different polymer chains, poly(methyl(2-(tris(2-H methoxyethoxy)silyl)ethyl)siloxane)) grafted with Si-tripodant centers (2550EO) known for their flexible structure was physically blended with poly(vinylidene fluoride-co-hexafluoropropylene (PVdF-HFP). Here, 2550EO containing varying amounts of amide salts ($LiF(SO_2CF_3)_2$ (LiTFSI)) was used as the main matrix. PVdF-HFP was used in concentrations of up to 30% to increase the film-forming ability of 2550EO/LiTFSI, and a series of solid polymer electrolyte (SPE) membranes were prepared. After incorporating the blended SPE with a minute amount of organic carbonates (only 15 wt%), the electrochemical features, such as Li^+ conductivity and transference number (t_{Li}^+), significantly increased. For example, a t_{Li}^+ of 0.42 and ionic conductivities of 0.64 and 0.3 $S\,cm^{-1}$ at 60 °C and 25 °C, respectively, were achieved. In addition, the electrochemical stability exceeded 5 and 4.8 V at 25 °C and 60 °C, respectively. Thus, a high Li/$LiFePO_4$ battery performance with high coulombic efficiencies exceeding 96% and 98% at 60 °C and 25 °C were achieved at 0.1 C, respectively. This was due to the superiority of the polysiloxane structure over its organic counterpart, attributed to its highly flexible backbone, high segmental mobility, and outstanding thermal and chemical stability.

Introduction

A method for maximizing the specific energy and energy density of lithium-ion batteries (LIBs) is to maximize the anode capacity. First, electrolyte systems should be considered to increase the possibility of using Li metal, which has a superior theoretical specific capacity (3860 $mAh\,g^{-1}$), as an anode material for next-generation battery technology to fulfill the increased energy, power, cycle life, and safety requirements.[1] In addition to the high risk of leakage, relatively low electrochemical stability, and the possible spontaneous combustion of organic liquid electrolytes, they are more reactive to Li metal.[2] Thus, solid electrolytes are considered the best alternatives to solve the internal short-circuit problem caused by lithium dendrites.[3,4] A type of solid electrolyte, organic solid polymer electrolytes (OSPEs), such as poly(ethylene oxide) (PEO)-, polyacrylonitrile (PAN)-, and poly(vinylidene fluoride) (PVdF)-based polymer electrolytes, have attracted attention because of their good contact and stability with Li metal anodes through their flexibility and mechanical strength.[5,6] However, they suffer from inherent limitations, such as the low Li^+ conductivity of $10^{-6}\,S\,cm^{-1}$ at 25 °C and the small Li^+ transference number ($t_{Li}^+ \approx 0.2$) of PEO-based OSPEs.[6,7] Oppositely, PVdF-based OSPEs have attracted significant interest owing to their high dielectric constant, good electrochemical stability, and sufficient mechanical intensity.[8] Moreover, the high T_g value and crystallinity of PVdF-based OSPEs have been partially reduced by introducing hexafluoropropylene (HFP) to PVdF to improve their ionic conductivity.[9] Although PVdF-HFP has been extensively studied as a polymer matrix for gel polymer electrolytes in LIBs, it is still not at the desired level for practical LIB applications.[10]

For SPEs, it is well-known that flexibility is critical for achieving high ionic conductivity.[7] We believe that flexible SPEs with high ionic conductivity can be achieved with a polysiloxane structure.[11,12] This is because, dissimilar to their organic counterparts, polysiloxanes possess a highly flexible backbone and high segmental mobility.[13] In addition, since siloxane polymers appear to be beneficial for critical solid electrolyte interphases (SEIs)[14,15] and are compatible with Li metal anodes,[16–18] they are competitive alternatives. Moreover, they are well-known for their durability at overcharge, high voltage, and are nonflammable even under harsh conditions[19] owing to their high antioxidative ability,[20] excellent thermal resistance,[21,22] and facile chemical modifications.[23–25] Li et al. first developed porous separators of polysiloxane/PVdF called "active separators" where PVdF was activated using polysiloxane (30% by weight) and used as a gel polymer electrolyte.[26] A Li salt liquid electrolyte was loaded after assembling the battery (cathode/separator/anode). The reported the liquid electrolyte uptake was 250 wt%, and the ionic conductivity of the obtained gel electrolyte membrane was $1.17\times10^{-3}\,S\,cm^{-1}$. Thereafter, Seidel et al. fabricated a hybrid polymer electrolyte

[a] Dr. A. Celik-Kucuk, T. Abe
Graduate School of Engineering
Kyoto University
Nishikyo-ku, Kyoto 615–8510 (Japan)
E-mail: asumancelikkucuk@gmail.com

Supporting information for this article is available on the WWW under https://doi.org/10.1002/batt.202300183

membrane comprising PVdF-HFP and ether-modified polysiloxanes.[27] Li et al. employed the cast film method, whereas Seidel et al. employed the airbrush spraying technique and obtained a thinner film and higher electrolyte update of 520 wt% but only achieved an ionic conductivity of 4.2×10^{-4} S cm^{-1} at 20 °C with PVdF-HFP and polysiloxane (20% by weight). Notably, both studies obtained the best results with membranes containing less than 30 wt% siloxane polymer, and the effect of the amount of siloxane on the outcome was not investigated. Recently, Bresser et al. blended a polysiloxane-based single-ion conductor (SIC) (PSiO; 50% by weight) with PVdF-HFP and fabricated flexible and self-standing polymer electrolyte membranes by solvent casting.[28] When they incorporated 57 wt% of organic carbonates, a Li^+ conductivity of 0.4 mS cm^{-1} and an electrochemical stability window of 4.8 V at 20 °C was achieved.

We recently reported the effectiveness of poly(methyl(2-(tris(2-H methoxyethoxy)silyl)ethyl)siloxane)) (2550EO) containing lithium bis(trifluoromethanesulfonyl)imide (LiTFSI) in suppressing Al current collector corrosion.[17] We observed that tris(2-H methoxyethoxy)silyl) (Si-tripodant centers) grafted on siloxane polymer, such as 2550EO, play important roles in increasing the t_{Li}^+ of the system and the electrochemical stability of the salt.[18] These results promoted the development of a self-standing solid electrolyte of 2550EO/LiTFSI and the use of the minimum required PVdF-HFP to ensure film formation. Therefore, we used 2550EO as the main polymer, PVdF-HFP as the co polymer, and LiTFSI salt as the Li source in the present study. However, dissimilar to the aforementioned studies, the present host matrix was 2550EO, which contained LiTFSI at varying ratios. Here, 2550EO was actively involved in the total ionic transport because it is a polymer containing Si-tripodant centers grafted onto the siloxane backbone. Furthermore, the addition of organic carbonate was maintained at an extremely low level (15 wt%) to ensure the mechanical intensity of the membrane and that the amount of combustible fractions remained low.

The physical blending of polymers with different molecular structures is a convenient modification strategy for improving ionic conductivity.[29] In addition, it is efficient and economical. Thus, a series of SPE membranes based on 2550EO/LiTFSI and PVdF-HFP were prepared in this study. The electrochemical performances, such as the ionic conductivity, Li-ion transference number (t_{Li}^+), and electrochemical stability window of these membranes with and without organic carbonates, were examined. The half-cell battery performance test of $LiFePO_4$ (LFP) with the blended 25500EO/LiTFSI + PVdF-HFP electrolyte membranes was also performed to obtain complementary information.

Experimental Section

Materials

The precursor, poly(methylhydrosiloxane) (trimethylsilyl terminated; average molar mass, 2550 g/mol); platinum divinyltetramethyldisiloxane (Pt(dvs), 3 wt% in xylene solution; Karlsted catalyst solution); a vinyl tris-2-methoxyethoxy silane monomer; and anhydrous toluene solvent were purchased from Aldrich Chemical Co. Inc. and used as received. LiTFSI electrolyte and a mixed solution of ethylene carbonate / propylene carbonate (EC/PC) (50/50 wt%) were purchased from Kishida Chemical Co., Ltd. (Osaka, Japan).

Synthesis of 2550EO

The siloxane-based polymer was prepared following reported procedures.[17,18,30] Poly(methylhydrosiloxane) (20 mL, 0.011 mol) was dissolved in anhydrous toluene (25 mL). Vinyl tris-2-methoxyethoxy silane (90 mL, 0.31 mol) and the 3% Karlsted catalyst solution in xylene (0.01 mL) were added, and the mixture was stirred at 50 °C. All the operations were conducted in an inert atmosphere. The structural characterization of 2550EO (Figure 1a) was confirmed by Fourier transform infrared (FTIR) and ^{1}H and ^{29}Si nuclear magnetic resonance (NMR), and the positional relationships between protons and silicon atoms were confirmed by two-dimensional (2D) NMR (^{1}H–^{1}H correlation spectroscopy (COSY) and ^{1}H–^{29}Si heteronuclear multiple bond correlation (HMBC)). The molecular weight of 2550EO has been determined by ^{1}H NMR spectroscopy to be $MW_{NMR} = 8720$ g mol^{-1}. The MW_{NMR} was considered during the electrolyte preparation. The density of 2550EO was determined to be 1.097 g mL^{-1} at 25 °C using an oscillating U-tube density meter (DMA 4500 M, Anton Paar GmbH).[17]

Electrolyte preparation

The water content of 2550EO was determined to be less than 10 ppm by coulometric Karl Fischer titration. The electrolytes were prepared in an argon-filled glove box (MBraun GmbH) with oxygen and water levels below 0.5 ppm by adding LiTFSI (EO/Li = 20, 10, and 5) to 2550EO. The mixtures were stirred at 25 °C for 2 days, and the resulting electrolyte solutions were labeled 20/1, 10/1, and 5/1 (Figure 1). The molar concentration of 20/1 has been reported to be 0.46 M.[15] The 20/1, 10/1, and 5/1 solutions (Figure 1a–c) were mixed with different amounts of PVdF-HFP dissolved in *N*-methyl-2-pyrrolidone (NMP) at RT (Table 1). First, 20/1 was blended with 9%, 15%, and 25% w/w PVdF-HFP and labeled 201#9, 201#15, and 201#25, respectively. Thereafter, 10/1 and 5/1 were blended with 30% and 28% w/w PVdF-HFP and labeled 101#30 and 51#28, respectively. The blended polymer electrolyte membranes were prepared using the solvent casting method. The solvent evaporated at 60 °C, followed by overnight vacuum drying at 80 °C. Images of the blended 2550EO + LiTFSI + PVdF-HFP electrolyte membranes (201#9, 201#15, 201#25, 101#30, and 51#28) are shown in Figure 1. PEO containing lithium bis(fluorosulfonyl)imide (LiFSI) (PEO/LiFSI) was prepared for comparison as a reference SPE in which the LiFSI content was 20/1 based on the EO/Li ratio. LiFSI (1 g) was dissolved in acetonitrile (CH_3CN, 30 g), and PEO (5 g) was gradually added to the solution and stirred for approximately 3 h at 25 °C. Thereafter, a known amount of the solution (depending on the desired thickness) was poured into a Teflon dish and dried in air for approximately 4–5 h at 80 °C for half a day and placed in a vacuum dryer at 80 °C overnight. Finally, 17.5-mm diameter membranes were punched out and placed in the glove box.

Characterization

The viscosity of the electrolytes (20/1, 10/1, and 5/1) was analyzed using a Lovis 2000 M viscometer (Figure S1a, Table S1). The solution structure was determined by Raman spectroscopy using

Research Article
doi.org/10.1002/batt.202300183
Chemistry Europe
European Chemical Societies Publishing

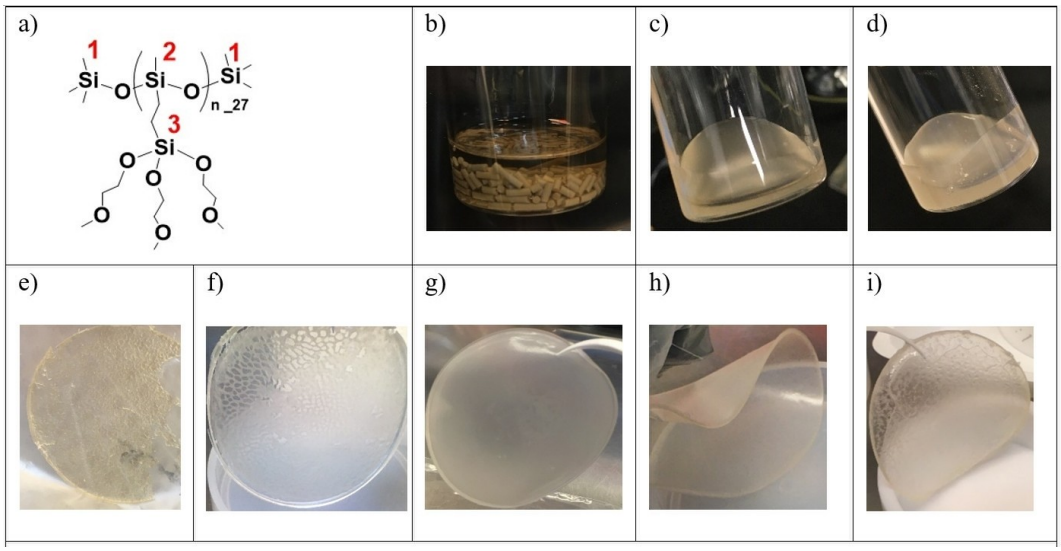

Figure 1. a) Structures of 2550EO. Images of 2550EO/LiTFSI at various EO/Li^+ ratios b) 20/1, c) 10/1, and d) 5/1 and blended 2550EO/LiTFSI + PVdF-HFP electrolyte membranes of e) 201#9, f) 201#15, g) 201#25, h) 101#30, and i) 51#28. (The undissolved columnar solids in (b) for 20/1 are molecular sieves added to absorb moisture, if any.)

Table 1. Comparison of the basic specifications of blended 2550EO/LiTFSI + PVdF-HFP electrolyte membranes of 201#9, 201#15, 201#25, 101#30, and 51#28 with 2550EO/LiTFSI electrolytes with different EO/Li ratios (20/1, 10/1, and 5/1) and a solid polymer electrolyte film of PEO/LiFSI at an EO/Li ratio of 20/1; conductivity, σ (S cm^{-1}) at 25 °C and 60 °C; E_a (kJ mol^{-1}), activation energy; Li transference number, $t_{Li}{}^+$. T_d = decomposition temperature

Polymer	Li salt	EO/Li w/w%	PVdF-HFP w/w%	Abbr.	σ [S cm^{-1}] 25/60 °C	$t_{Li}{}^+$	$E_{a\sigma}$	$T_{d,5\%}$ [°C][a]
2550EO	LiTFSI	20/1 (REF)[17]	–	20/1	$5.0\times10^{-5}/1.5\times10^{-4}$	0.33	25	~305
2550EO	LiTFSI	10/1	–	10/1	$8.1\times10^{-5}/2.8\times10^{-4}$	0.27	27	~305
2550EO	LiTFSI	5/1	–	5/1	$6.4\times10^{-5}/3.4\times10^{-4}$	0.33	37	~305
2550EO	LiTFSI	20/1	9	201#9	$2.3\times10^{-5}/6.4\times10^{-5}$	0.37	24	~335
2550EO	LiTFSI	20/1	15	201#15	$1.9\times10^{-6}/7.4\times10^{-6}$	0.33	31	~335
2550EO	LiTFSI	20/1	25	201#25	$5.9\times10^{-7}/3.0\times10^{-6}$	n.a.	37	~335
2550EO	LiTFSI	10/1	30	101#30	$1.3\times10^{-5}/2.8\times10^{-5}$	0.14	27	~335
2550EO	LiTFSI	5/1	28	51#28	$8.7\times10^{-5}/2.9\times10^{-4}$	0.28	28	~335
PEO	LiFSI	20/1	–	PEO/LiFSI	$1.5\times10^{-7}/2.0\times10^{-4}$	0.19	n.a.	REF[6]

[a] The temperature at which the weight loss of the sample was 5 %.

an NRS-5100 spectrometer (Jasco) at a laser excitation wavelength of 532 nm (Figures S1b and c). The glass transition temperature (T_g) was measured by differential scanning calorimetry (TA Q100) at a heating and cooling rate of 10 °C min^{-1} across the temperature range of −80 to 180 °C. The crystallinity of the polymer membrane was evaluated using Equation (1):

$$X_c = \frac{\Delta H_m}{\Delta H_{m^0}} \quad (1)$$

where $\triangle H_m$ is the melting enthalpy of the sample, and $\triangle H_m{}^\circ$ is the melting enthalpy of a 100 % crystalline sample of pure PVdF (104.6 J g^{-1}).[31] Thermogravimetric analysis (TGA) was performed using a TA Q50 at a heating rate of 10 °C min^{-1} in an N_2 atmosphere from RT to 500 °C (Figure S2a). The surfaces of the prepared membranes were analyzed by field-emission scanning electron microscopy (FE-SEM, SU-8020) and energy-dispersive X-ray (EDX) spectroscopy (Hitachi High-Technologies, province, country).

Electrode preparation

Here, electrochemical tests were conducted using CR2031-type coin cells. For the cathode, 85 wt% LFP active material, 10 wt% PEO containing 15 % LiFSI as a binder, and 5 wt% acetylene black (Denka Black Li-100, Denka Co., Ltd., Tokyo, Japan), as an electron-conducting agent, were mixed with CH_3CN (Sigma Aldrich). The slurry was coated onto a carbon-coated Al foil (Al_C; 15-μm thickness) with a mass loading (LFP) in the range of 1.0–2 mg cm^{-2} and heated at 80 °C for 8 h. The cells were assembled in an argon-filled glove box with Li foil (300-μm thickness) functioning as a counter electrode. During the assembly, the cathodes were first placed on the surface of a stainless cover, then the blended polymer electrolyte membrane was placed on it and sealed with Li metal (300-μm thickness) (Scheme S1a). The blended polymer electrolyte membrane was soaked in ~50 μL of EC/PC for 10 min prior to battery construction.

Electrochemical characterization

The ionic conductivities were measured by alternating current (AC) impedance spectroscopy (Solartron 147055BEC, Solartron Analytical) over a frequency range of 0.1–10^6 Hz at an amplitude of

10 mV. The blended SPE was sandwiched between two stainless-steel (SS) blocking electrodes to construct SS/electrolyte/SS (Scheme S1b). The resistance was determined using Equation (2):

$$\sigma = {}^{L}/_{RS} \quad (2)$$

where L, R, and S are related to the thickness of the blended SPE, total resistance, and area of the free-standing SPE, respectively. The correct thickness of the membrane (thickness after the disassembly of the SS/SS coin cell) was considered for the calculation. Although the thicknesses of 101#30 and 201#25, after the disassembly of the SS/SS coin cell, remained practically unchanged, compared with their initial thicknesses (a thinning from the ranges of 110–190 to 110–180 μm), the initial thickness of PEO/LiTFSI, which was approximately 600–650 μm, decreased to a range of 140–170 μm after the SS/SS coin cell was disassembled. The cells were thermostated using a Vötsch climatic chamber, and the conductivity was conventionally calculated by fitting the corresponding Nyquist plots.

Li-ion transference number measurements were conducted using a Li | blended 2550EO/LiTFSI + PVdF-HFP electrolyte membrane | Li-battery system polarized with a direct current (DC) voltage of 10 mV (Scheme S1c). The Li-ion transference number was determined using the Bruce-Vincent formula[32] in Equation (3) as follows:

$$t_{Li^+} = \frac{I_{ss}(\Delta V - I_0 R_0)}{I_0(\Delta V - I_{ss} R_{ss})} \quad (3)$$

where ΔV is the potential applied across the battery (10 mV in this case); I_0 and I_{SS} are the initial and steady-state currents, respectively; and R_0 and R_{SS} are the initial and steady-state interfacial resistances of the passivating layers of the Li metal electrodes, respectively. The conductivity and transference number were measured several times, and the average values were determined.

The electrochemical window of the blended SPEs was evaluated by linear sweep voltammetry (LSV) at a scan rate of 1 mV s^{-1} with CR2031 coin cells comprising SS as a working electrode and Li metal as the reference and counter electrodes (Scheme S1d). The prepared SPEs were subjected to LSV experiments using the Solartron at potentials ranging from the open-circuit voltage (OCV) to 5.5 V (at 25 °C and 60 °C) (vs. REF) at a sweep rate of 1 mV s^{-1}. Electrochemical measurements were performed using a Hokuto Denko HJ1001SD8 system. Galvanostatic charge-discharge cycling tests were also conducted using the Hokuto Denko HJ1001SD8 system at 25 °C or 60 °C in the Vötsch thermostatic chamber. The Al corrosion of a Li/Al_C (Al_C; carbon-coated Al) two-electrode CR2031 coin cell was tested using the potential-step method.

Results and Discussion

Polysiloxanes grafted with Si-tripodant centers (2550EO) with LiTFSI salts at various EO/Li$^+$ ratios of 20/1, 10/1, and 5/1 were prepared. The resulting electrolyte solutions were labeled 20/1, 10/1, and 5/1; 10/1 and 5/1 were prepared for the first time in the present study. As shown in Figure 1, 20/1 was liquid, 10/1 was a viscous liquid, and 5/1 was in a liquid wax state. Although the dynamic viscosities of 20/1 and 10/1 were practically the same, almost a three-fold increase was observed for 5/1 (Table S1, Figure S1a). Although the ionic conductivity of neat 5/1 at low temperatures was slightly higher than that of 10/1, 10/1 exhibited a slightly higher ionic conductivity at high temperatures (Table S2), probably because of the higher viscosity of 5/1. The Raman spectra of 10/1 and 5/1 were compared to those of 20/1 in Figure S1(b) and exhibited a complex formation of EO units with Li that was observed as a shoulder at 854 cm^{-1}. For 5/1, this shoulder was wide and visible. The intensity of the band at 739 cm^{-1} attributed to "free TFSI anions" or solvent-separated ion pairs reduced, whereas that of the band at 745 cm^{-1} attributed to contact ion pairs or aggregates increased with an increase in the salt concentration (Figure S1c).

To improve the film-forming ability and insufficient ion transport capacity of PVdF-HFP, 20/1, 10/1, and 5/1 were physically blended with varying PVdF-HFP concentrations.[10] The 2550EO polymer possesses an extremely flexible backbone, and its ion transport efficiency has been confirmed.[13,17] Detailed information is provided in the Experimental Section and Table 1.

Images of the blended 2550EO/LiTFSI + PVdF-HFP electrolyte membranes (201#9, 201#15, 201#25, 101#30, and 51#28) are shown in Figure 1(d–h). 201#9, 201#15 and 201#25 membranes prepared by mixing of 20/1 with 9%, 15% and 25% w/w PVdF-HFP, respectively. On the other hand, 101#30 and 51#28 membranes were prepared by mixing of 10/1 and 5/1 with 30% and 28% w/w PVdF-HFP, respectively. Figure 1 demonstrates that free-standing films with homogeneous morphology, good ductility, and mechanical strength were obtained for 201#25 and 101#30.[33] However, 201#9, 201#15, and 51#28 exhibited low film-forming abilities. The low PVdF-HFP ratio was insufficient to form a self-standing film for 201#9 and high-quality film morphology for 201#15 while a high LiTFSI content in 51#28 resulted in the crystallization of LiTFSI. As shown in Figure S2(a), the decomposition temperature of the blended SPE systems exceeded 335 °C because of the temperature stability of PVdF-HFP (approximately 475 °C)[34] and polysiloxane (> 300 °C).[17]

A slight decrease was observed in the ionic conductivity of 201#9 compared to 20/1. However, for 201#15, a large decrease was observed in the ionic conductivity, which continuously decreased with the addition of up to 25% PVdF-HFP (201#25). Although the presence of PVdF-HFP improved the film morphology, the high PVdF-HFP concentration probably triggered a blocking effect for the membranes containing 20/1. This behavior might be attributed to the lack of Li$^+$ carriers due to the extremely low LiTFSI content in the EO/Li:20/1 electrolyte system. Conversely, compared to 10/1, a relatively small decrease was observed in the ionic conductivity of 101#30 with a high LiTFSI content. In addition, practically no change was observed in the conductivity of 51#28 (the sample with the highest salt content). Thus, the role of PVdF-HFP on the blocking effect for the membrane was observed to be less in 101#30 and practically nonexistent in 51#28 with a sufficiently high salt content. This result is simply attributed to the increase in the number of mobile ions with the addition of more salt.

PEO/LiFSI was prepared as a reference SPE in which the LiFSI content was 20/1 based on the EO/Li ratio (Figure S2d).

Research Article
doi.org/10.1002/batt.202300183
Chemistry Europe
European Chemical Societies Publishing

The ionic conductivities of 201#9, 201#15, and 201#25 at 25 °C were considerably higher than that of PEO/LiFSI at the same salt concentration of 20/1:EO/Li (Figure S2b and Table S3). However, it is well-known that the ionic conductivity of PEO-based polymer electrolytes substantially increases within the range of 40–50 °C (Figure S2d), which correlates with the T_g of PEO dissolved with Li salts.[5] Therefore, the conductivity of PEO/LiFSI at 60 °C was significantly higher than those of 201#9, 201#15, and 201#25. Notably, 201#9, 201#15, and 201#25 were considered here for comparison, and these membranes had salt densities that were relatively lower than that of PEO/LiFSI since they contained PVdF-HFP. At low temperatures (below 50 °C), 101#30 and 51#28 exhibited high ionic conductivities similar to those of PEO/LiFSI at high temperatures above 60 °C. Thus, σ changed in the order of 5/1 ~ 51#28 > 10/1 > PEO/LiFSI > 101#30 > 201#9 > 20/1 > 201#15 > 201#25 at 60 °C. The trend at 25 °C was in the order of 51#28 > 10/1 > 5/1 > 20/1 > 201#9 > 101#30 > 201#15 > 201#25 > PEO/LiFSI (Figure S2b). As can be seen, except for 51#30, the ionic conductivities of the solid membranes are lower than 20/1, 10/1 and 5/1. High interfacial resistance was probably responsible for the low ionic conductivity of the solid membranes. Therefore, to solve this problem, liquid organic carbonate, for surface treatment, was introduced into the siloxane/PVdF-HFP blended system to increase the wetting, reduce the interfacial resistance, and directly increase the ionic conductivity. An organic carbonate blended system of the EC/PC solvent mixture was selected because of its particularly stable combination toward oxidation in a high voltage region.[35]

After incorporating EC/PC into the siloxane/PVdF-HFP blended systems, electrochemical features such as ionic conductivity (Figure 2), E_a (Table 1), and t_{Li}^+ (Table S6 and Figures S3 and S4) significantly improved, particularly for 201#25 and 101#30. As shown, the increase in the ionic conductivity of 201#25/EC/PC and 101#30/EC/PC was extremely higher than those of 201#9/EC/PC and 201#15/EC/PC. For example, the ionic conductivity of 201#25/EC/PC was two orders of magnitude higher at almost all temperatures compared with that of 201#25. The ionic conductivity of 101#30/EC/PC was the most promising. For example, by introducing EC/PC into 101#30, the ionic conductivities of 0.63 and 0.32 mS cm^{-1} at 60 °C and 25 °C were achieved, respectively. These values were approximately three and two orders of magnitude higher than that of neat 101#30, respectively (Figure 2b). In addition, the ionic conductivity of 101#30/EC/PC was four and three times higher at 25 °C and 60 °C, respectively, compared with that of 10/1, which was a viscous liquid and did not contain PVdF-HFP. Compared with the estimated required conductivity of 10^{-3} S cm^{-1} for practical purposes at the operating temperature, 101#30/EC/PC particularly exhibited an extremely promising ionic conductivity (Table 2).

For 201#9, 201#15, 201#25, 101#30, and 51#28, the variation in conductivity with temperature was mainly fitted using Arrhenius-type equations (Figure 2a and b), which are described below [Eqs. (4) and (5)]:

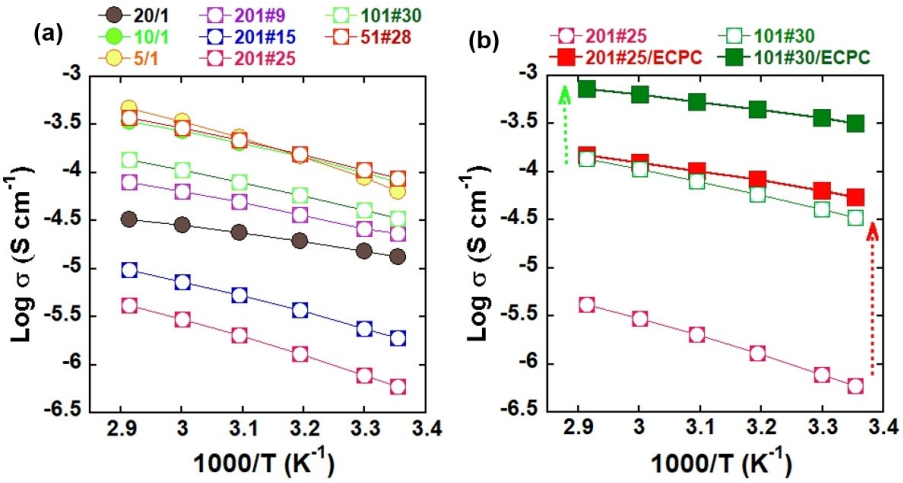

Figure 2. Temperature-variable ionic conductivity of 20/1, 10/1 5/1, and the blended 25500EO/LiTFSI + PVdF-HFP electrolyte membranes of 201#9, 201#15, 201#25, 101#30, and 51#28 a) without and b) with EC/PC.

Table 2. Basic specifications of EC/PC-introduced blended 25500EO/LiTFSI + PVdF-HFP electrolyte membranes of 201#9, 201#15, 201#25, and 101#30; conductivity, σ (S cm^{-1}) at 25 °C and 60 °C; E_a (kJ mol^{-1}), activation energy; and Li transference number, t_{Li}.

Polymer	Li salt	EO/Li w/w%	PVdF-HFP w/w%	EC/PC amount [μL]	Abbr.	σ at 25 °C/60 °C [S cm^{-1}]	t_{Li}^+	$E_{a\sigma}$
2550EO	LiTFSI	20/1	9	+50	201#9/EC/PC	1.9×10^{-4}/3.6×10^{-4}		14.2
2550EO	LiTFSI	20/1	15	+50	201#15/EC/PC	7.8×10^{-5}/1.8×10^{-4}		18.3
2550EO	LiTFSI	20/1	25	+50	201#25/EC/PC	5.5×10^{-5}/1.3×10^{-4}	0.23	19
2550EO	LiTFSI	10/1	30	+50	101#30/EC/PC	3.2×10^{-4}/6.3×10^{-4}	0.42	15.4

Research Article
doi.org/10.1002/batt.202300183
Chemistry Europe
European Chemical Societies Publishing

$$\ln(\eta) = ln(A_s) + \frac{E_a}{R}\left(\frac{1}{T}\right) \quad (4)$$

$$\ln(\sigma) = ln(A_s) + \frac{E_a}{R}\left(\frac{1}{T}\right) \quad (5)$$

where R, E_a, and A_s are the gas constant (8.31 JK^{-1} mol^{-1}), Arrhenius activation energy, and preexponential (entropic) factor of the Arrhenius equation for liquid systems, respectively. It is well-known that an Arrhenius-type behavior ($\sigma T \sim \exp(-E_A/k_BT)$) indicates that relaxation dynamics follow purely thermally activated processes, during which the relaxing units overcome known potential barriers.

As shown in Table S6 and Figures S3 and S4, the t_{Li}^+ of 101#30/EC/PC increased from 0.14 to 0.42, which was higher than those of the other siloxane-based blended membranes and even considerably higher than that of a reported liquid electrolyte (0.35).[36] Therefore, owing to the higher ionic conductivities of 201#25/EC/PC and 101#30/EC/PC and the promising t_{Li}^+ of 101#30/EC/PC (Figure S4), only 201#25/EC/PC and 101#30/EC/PC were further evaluated. In addition, as shown in the image obtained after introducing EC/PC into PEO/LiFSI, the PEO/LiFSI SPE (Figure S2e) dissolved in EC/PC (Figure S2f). Therefore, it was impossible to compare the EC/PC-introduced siloxane/PVdF-HFP and PEO/LiFSI systems.

Figure 3(a, b) and (g, h) shows the surface morphologies of 201#25 and 301#30, respectively. The SEM images show that PVdF-HFP was uniformly dispersed in the polysiloxane matrix in 101#30, resulting in a smooth film morphology. However, aggregates were separated from each other by boundaries in 201#25. F, Si, and S atoms were available in PVdF-HFP, 2550EO, and LiTFSI, respectively; therefore, EDX mapping analysis was performed to determine their distribution in the electrolyte system. Although 2550EO and PVdF-HFP were segregated in 201#25 (Figure 3c–f), their distribution was uniform in 101#30 (Figure 3i–l). Therefore, the boundaries in 201#25 inhibited ion mobility. This was probably a major reason for the relatively lower ionic conductivity of 201#25 compared with that of 101#30. PVdF-HFP exhibited poor miscibility with 2550EO in 201#25, whereas it exhibited good miscibility with 2550EO in 101#30. We believe that the good miscibility of PVdF-HFP with 2550EO in 101#30 was due to the ion-polymer interaction (Lewis acid and base) between Li^+-$TFSI^-$ and PVdF-HFP and the relatively higher LiTFSI content in 101#30. This approach is in agreement with the literature.[37,38]

Figure 4(a) shows the X-ray diffraction (XRD) patterns of PVdF-HFP, 201#25, and 101#30. It has been reported that the

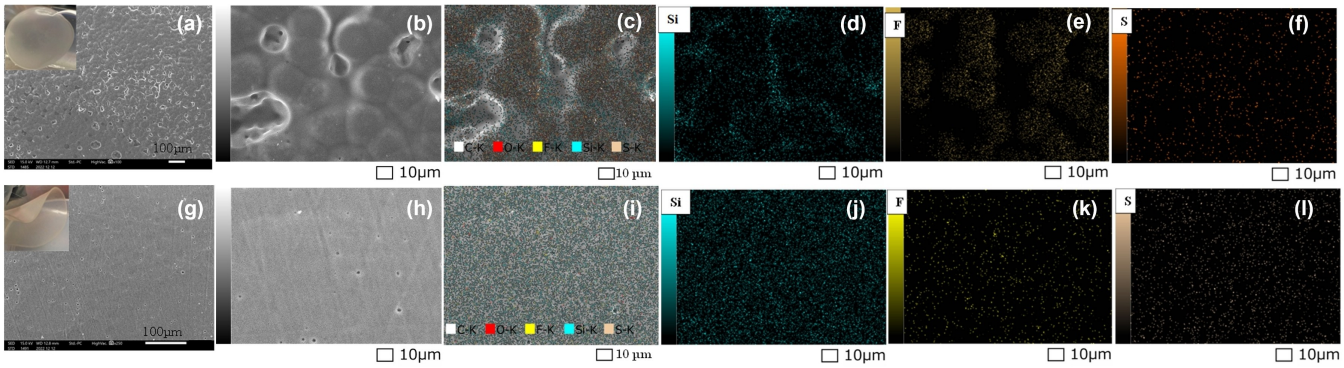

Figure 3. Surface FE-SEM images of a, b) 201#25 and g, h) 301#30. EDX mappings of c–f) 201#25 and i–l) 301#30, d, j) Si, e, k) F, and f, l) S.

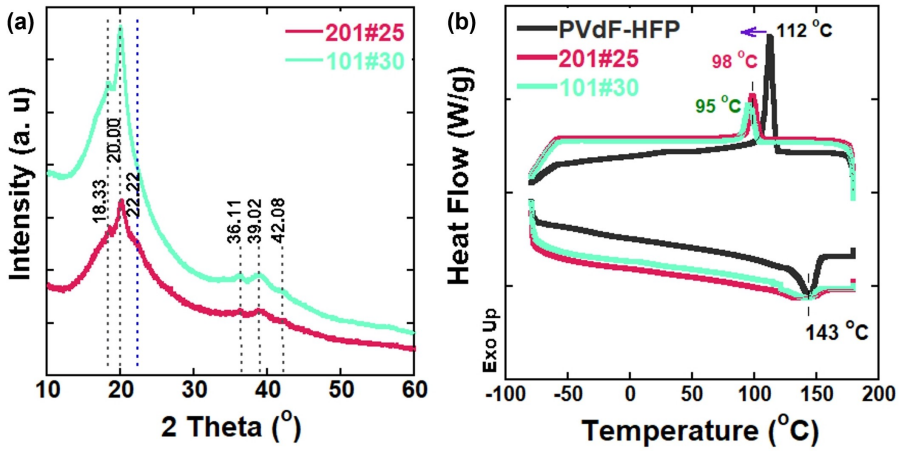

Figure 4. a) XRD patterns of 201#25 and 101#30. b) DSC thermograms of 201#25, 101#30, and PVdF-HFP.

Research Article
doi.org/10.1002/batt.202300183
Chemistry Europe
European Chemical Societies Publishing

PVdF-HFP film exhibits diffraction peaks at 18.5°, 20.0°, 26.5°, and 39.0° related to the α-crystal PVdF-HFP chain.[39] Here, 201#25 exhibited diffraction peaks at 18.2°, 20°, 22.1°, 36.4°, 38.9°, and 42.2°. These diffraction peaks were also observed for 101#30, except for the diffraction peak at 22.1°. Considering the homogeneous distribution among the blended components in the SEM and mapping analyses of 101#30, the absence of the diffraction peak at 22.1° might be because the crystallization of PVdF could be partially suppressed. In addition, no intense peak related to the crystalline nature of LiTFSI,[40] which was reported at 13.6°, 15.9°, 18.6°, 18.9°, and 21.4°, was observed because LiTFSI was fully complexed first with 2550EO and with PVdF-HFP, particularly in 101#30. The DSC measurements shown in Figure 4(b) correlated with the XRD results. The crystallinity degree of PVdF-HFP (26.3%) reduced after blending with 2550EO/LiTFSI (Figure S5). As the characteristic endothermic peak at approximately 143 °C related to the melting temperature of PVdF-HFP decreased, the melting peak area also significantly decreased. The crystallinity of PVdF-HFP in 201#25 and 101#30 was approximately 10%. Sousa et al. reported that the crystallinity of PVdF-HFP was in the range of 15%–35%;[31] the obtained X_c (10%) was lower than this range. Although there was not such a clear difference between 201#25 and 101#30, compared with pure PVdF-HFP, their crystallinity significantly reduced. This reduction confirmed the amorphous morphologies of 201#25 and 101#30. However, a more amorphous and smooth morphology was achieved for 101#30, probably due to the better compatibility between PVdF-HFP and polysiloxane in 101#30, as revealed by SEM. The smoother morphology of 101#30 probably resulted in a more homogeneous EC/PC diffusion. In addition, the polymer chains in the amorphous region exhibit an extremely flexible structure, thereby increasing the Li-ion conductivity by promoting the segmental movement of the polymer chain, which explained the high ionic conductivity (0.32 mS cm^{-1}) and high t_{Li^+} (0.42) of 101#30. It is believed that more free mobile Li ions formed because of the homogeneous EC/PC diffusion in 101#30, which enabled the break-up of the ion-pair clusters (Li^+-$TFSI^-$) and reduced the Lewis acid-base interaction between Li^+ and PVdF-HFP.[37,38]

The reversible electrochemical plating/stripping behavior of Li in 10/1 and 5/1 was practically identical at 25 °C (Figure S6a), as previously reported for 20/1. Two redox peaks were observed at approximately 0 V (vs. Li^+/Li), indicating the reversible Li dissolution/deposition process on the SS electrode with no other current peak. LSV was applied (2–6 V) to test the electrochemical stability of 10/1 and 5/1 with a Li anode at 25 °C and 60 °C (Figure S6b). As shown, they were both durable at approximately 5 and 5.5 V at 60 °C and 25 °C, respectively. The low electrochemical stability of the salt (< 4.2 V vs. Li/Li^+) almost disappeared for 5/1, probably because of the stabilization of the TFSI anion through stable anion-driven passivation. It was confirmed that LiTFSI-based Al current collector corrosion was completely suppressed in the siloxane systems with high salt concentrations (10/1 and 5/1) as in the system with a low salt concentration (2550EO/LiTFSI; EO/Li:20/1) (Figure S7).

Figure 5(a) shows that the incorporation of polysiloxane with PVdF-HFP for 201#25 and 101#30 did not significantly affect the promising electrochemical stability of all the systems at 60 °C. The siloxane structure stabilized the system against the low oxidation stability of the salt in 201#25. However, by increasing the LiTFSI salt content in 101#30, low electrochemical stability was observed for the salt (vs. Li/Li^+) at potentials above 3.5 V. This might have been because the low siloxane content of 101#30 was insufficient to suppress the electrochemical instability of the salt. Fortunately, EC/PC improved the stability of the salts in 101#30 and 201#25. The electrochemical stability of 201#25/EC/PC and 101#30/EC/PC exceeded 5 and 4.8 V at 25 °C and 60 °C, respectively (Figure 5b). This was probably because the EC/PC system created a stable SEI on the electrode surface without further degradation of the electrolyte system.[40,41] Although irrelevant here, we believe that the improvement in passivation film quality warrants further study.

Next, 101#30/EC/PC was examined for a thin-film battery system to investigate its compatibility with the battery test.

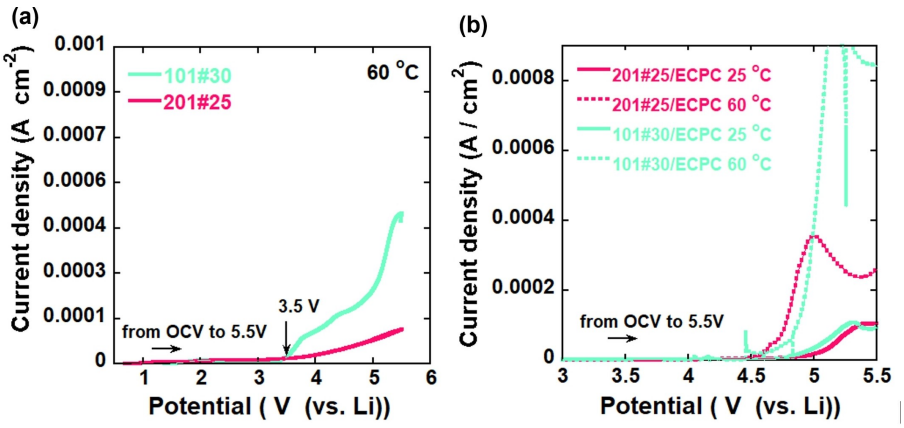

Figure 5. Electrochemical stability window of the Li/SS cell through linear sweep voltammetry (LSV) from OCV to 5.5 V vs. Li/Li^+ for the blended 25500EO/LiTFSI + PVdF-HFP electrolyte membranes of 201#25 and 101#30 a) without and b) with EC/PC.

Research Article
doi.org/10.1002/batt.202300183
Chemistry Europe
European Chemical Societies Publishing

Therefore, the half-cell battery test of the LFP cathode was tested with the 201#25, 101#30, 201#25/EC/PC, and 101#30/EC/PC electrolyte systems. Coin-type cells were assembled using a metallic Li anode and LFP cathode. The cutoff voltage range was 2.5–3.9 V. The first five cycling behaviors of 201#25 and 101#30 at 60 °C and 0.1 C are shown in Figure S8(a, b). The LFP/Li-battery performances of 101#30 and, in particular, 201#25, were unstable and gradually decreased as the cycles proceeded. It is believed that insufficient contact with the electrode caused high interfacial resistance; thus, the low ionic conductivity was the main reason for this result.

Figure 6(a) shows the first charge-discharge voltage curves of the LFP/Li half cells at 60 °C and 0.1 C. The initial discharge capacities of 201#25 and 101#30 were 60 and 80 mAh g^{-1}, respectively, whereas those of 201#25/EC/PC and 101#30/EC/PC almost reached 120 and 150 mAh g^{-1}. After 20 cycles, the capacity of 201#25/EC/PC remained at 120 mAh g^{-1} at 60 °C, which was related to a capacity retention of 80%. Oppositely, the capacity improvement was large for 101#30/EC/PC; therefore, the cycling performances of 101#30/EC/PC were elaborately examined at 25 °C and 60 °C (Figure 6b). The initial discharge capacity of 101#30/EC/PC was 140 and 146 mAh g^{-1} at 25 °C and 60 °C, respectively. After 30 cycles, the capacity reduced to 125 and 120 mAh g^{-1} at 25 °C and 60 °C, with capacity retentions of 90% and 82%, respectively. The coulombic efficiency exceeded 99% at 25 °C and was approximately 95% at 60 °C, demonstrating the promising cycling performance of 101#30/EC/PC, particularly at RT (25 °C).

To demonstrate the effectiveness of the LiTFSI-containing siloxane-based SPE system, we examined the LiTFSI-based SPE (PEO/LiFSI; EO/Li, 20/1) and carbonate-based liquid electrolyte as a reference (1 M LiTFSI/PC) for the same battery system. As illustrated in Figure 6(b), the capacity of LFP/Li with the PEO/LiFSI SPE at 60 °C was significantly insufficient, with a discharge capacity of only 120 mAh g^{-1} compared with 146 mAh g^{-1} of 101#30/EC/PC at 60 °C. The battery performance of PEO/LiFSI at 60 °C correlated with that of a relevant study.[42] Furthermore, LFP/Li with PEO/LiFSI could not be operated at 25 °C because of the extremely low ionic conductivity of the PEO/LiFSI SPE at temperatures below the T_g of PEO.[3] As previously mentioned, since the PEO polymer is subject to dissolution in EC/PC, surface treatment with EC/PC was not employed to eliminate the risk of short-circuiting the battery system. Oppositely, although the performance of LFP/Li in 1 M LiTFSI/PC exhibited the highest capacity of 157 mAh g^{-1} at 60 °C, a capacity retention of only 61% for 30 cycles and a significant capacity fading as the cycles proceeded was observed. A poor capacity of 120 mAh g^{-1} at 25 °C was also observed.

The promising cycling stability of 101#30/EC/PC was attributed to the remarkable Li stability of 265 μA cm^{-2} (Figure S9a) and the long-term Li stability/compatibility of the siloxane structure in 2550EO/LiTFSI (10/1) at a current density of 0.06 mA cm^{-2} (Figure 7a). However, the Li stability/compatibility of 2550EO/LiTFSI (20/1) can last for approximately 400 h at a current density of 0.01 mA cm^{-2} (Figure S9c). Furthermore, current density as a function of voltage was examined for the electrolyte membranes of 201#25 and 101#30, and the relevant results are shown in Figures 7(b), S9(b and d), respectively. The voltage was scanned in a staircase progression from 0 to 1.1 V vs. Li/Li$^+$, and the resultant current behavior was examined. For 201#25, a steady-state current (3.3 μA) of up to 0.5 V was achieved probably because of the over-limiting conduction, which resulted in instability. A clear plateau region was observed for 101#30, indicating that a steady-state current was reached for each increased voltage (Figure S9b). The current density first increased to 18 μA and appeared to have been stabilized by the diffusion-limiting current even up to a fairly high voltage (1.1 V). We hypothesize that the Lewis acid-base interaction (between Li$^+$ and PVdF-HFP) in 101#30 was sufficiently strong to ensure the good miscibility of PVdF-HFP and sufficiently weak to allow ion transport. We believe that the LiTFSI content in siloxane/PVdF-HFP systems plays an important role in morphology and ion transport. Therefore, although 101#30 suppressed instability during electrodeposi-

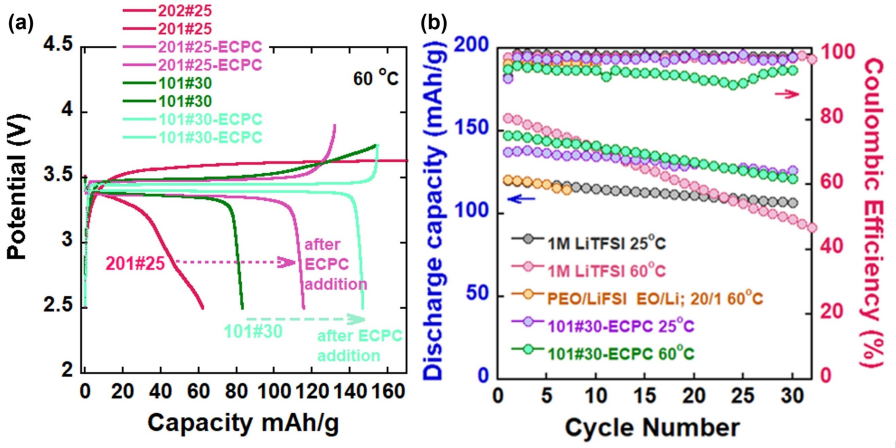

Figure 6. a) First charge/discharge profiles of LFP/Li cells with the blended 25500EO/LiTFSI + PVdF-HFP electrolyte membranes of 201#25 and 101#30 without and with EC/PC at 60 °C. b) Cycling stability comparison of LFP/Li cells with 101#30-EC/PC at 25 °C and 60 °C, PEO/LiFSI EO/Li:20/1 at 60 °C, and 1 M LiTFSI in PC at 25 °C and 60 °C. All the measurements were performed at a rate of 0.1 C. The accurate thickness range of the 101#30 and PEO/LiFSI electrolyte membranes was 110–180 μm during the performance test.

Research Article
doi.org/10.1002/batt.202300183
Chemistry Europe
European Chemical Societies Publishing

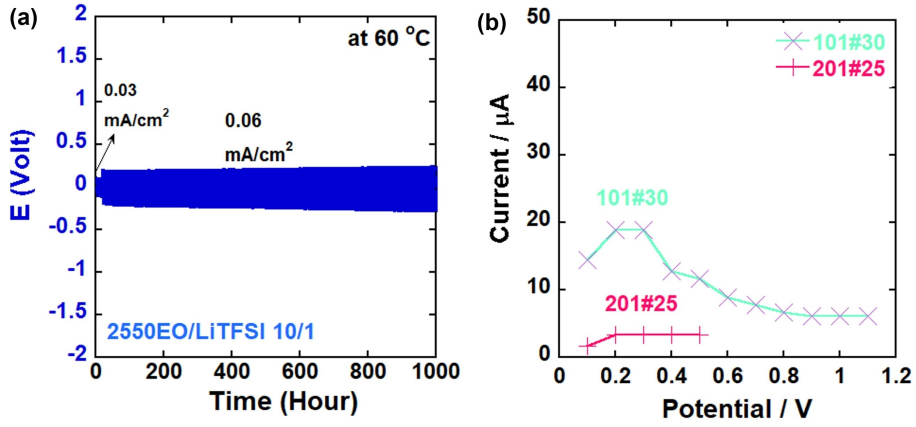

Figure 7. a) Long-term cycling of symmetrical Li–Li cells with 2550EO/LiTFSI electrolytes at an EO/Li^+ ratio of 10/1 at 0.06 mA cm^{-2} and 60 °C. b) Current as a function of voltage for 101#30 at 60 °C.

tion (Figure 7b), 201#25 could not because the ion transport rate at every potential difference could not be a function of ionic conductivity.

Furthermore, we investigated the mechanical and peeling properties of 101#30 in relation to this promising cycling stability. A Li/LFP coin cell with a 101#30/EC/PC membrane was prepared and maintained at 60 °C for 3 h, then the coin cell was disassembled. Figure S10(a) shows an image of the disassembled Li/LFP coin cell with a 101#30/EC/PC membrane. The 101#30 membrane was gently peeled off and washed several times with EC/PC. As shown in Figure S10(b), the membrane was easily peeled off the Li metal, and the LFP composite cathode. 101#30 membrane maintained almost the same shape and thickness as that of the initial state. This was attributed to the good mechanical strength of 101#30. Next, the organic carbonate uptake ability of 101#30 was investigated. Four 101#30 electrolyte membranes were immersed in EC/PC for 30 min. The average EC/PC uptake of 101#30 was observed to be 15%, which was very low compared with those of previous studies.[10,28] As previously mentioned, only 50 μm EC/PC was applied to the electrolyte membranes. Considering the uptake capacity of 101#30 (15 wt%), it would not be wrong to describe 101#30/EC/PC as a solid-like membrane but not a gel electrolyte system. We believe that the low EC/PC uptake led to a lack of swelling of the membrane and, thus, did not cause a decrease in the membrane strength as seen in Figure S10. It is thought that the applied EC/PC only played a role in providing good contact at the electrolyte-electrode interface and creating a stable SEI on the electrode surface.

To eliminate the flammable hazard of EC/PC, only a small amount (50 μL) was used. In addition, EC/PC uptake capacity of 101#30 is very low (15 wt%). However, remarkable improvements were achieved. The application of an extremely minimal amount of EC/PC is important for nonflammability criteria of the system and is one of the main factors that differentiate the present study from previous studies based on polysiloxane/PVdF blended membranes.[24–26] On the other hand, the minimal amount of organic carbonate (EC/PC) seems well enough to ensure good contact between membrane and electrodes. Thus, it is clear that this work sheds light on the development of fully solid-state cells (Figure S10) with acceptable ionic conductivity (0.3 mS cm^{-1} at RT), wettability and low cost. In particular, we considered that the performance of the SPE could be optimized by testing different organic carbonate systems and the applied process, as it is highly probable that the results obtained here will considerably improve. The ionic conductivity of the proposed membrane was promising. The synergistic effect of the aforementioned factors and its high oxidative stability (> 5 V) accelerate its potential for use as an SPE in high voltage cathode systems and warrant further studies. Thus, a future study on optimization is required.

Conclusions

Here, 2550EO was blended with different ratios of LiTFSI and PVdF-HFP, and a series of SPE membranes were prepared. Although their high oxidative stabilities remained unchanged, outstanding ionic conductivity and t_{Li}^+ were achieved after incorporating the blended SPE with a small amount of EC/PC (15 wt%). In particular, 101#30/EC/PC exhibited an ionic conductivity of 0.3 mS cm^{-1}, a t_{Li}^+ of 0.42 at RT, and a wide electrochemical stability window of over 5 V. Thus, a high Li/LFP battery performance with a high coulombic efficiency of over 99% at RT was achieved at 0.1 C. This was attributed to the highly flexible backbone, high segmental mobility, and superior thermal and chemical stability of the polysiloxane structure.

The stable thermal and electrochemical properties of siloxane-based electrolytes render them excellent candidates for RT LIB applications. Therefore, we strongly believe that polysiloxane-based materials can play practical roles in LIBs. Testing different organic carbonates to soften solid polymer blends and testing these blended membranes with high voltage cathode active materials, particularly 101#30, require further studies.

Supporting Information

Some additional analysis related to thermal gravimetry measurements, ionic conductivity measurement for PEO-based reference solid polymer electrolyte of PEO/LiFSI (EO/Li; 20/1), viscosity measurements, electrochemical impedance spectroscopy (EIS), chronoamperometry test of Al (Al/Li) in the presence of high salt-concentrated siloxane-based electrolyte (2550EO/LiTFSI, EO/Li; 10/1 and 5/1) have been provided as Electronic Supporting Information (EIS).

Author Contributions

Asuman Celik-Kucuk: Conceptualization, Investigation, Writing-Original Draft, Writing-Review & Editing, Visualization. Takeshi Abe: Project administration, Funding acquisition

Acknowledgements

This work was supported by the "System Design of Solid Type Battery" project of university-industrial collaboration (Kyoto University-Sumitomo Chemical), Japan. [grant numbers 150190900253]. The authors thank Izumi Yamada for the EIS measurements and Prof. Kazuhiko Matsumoto, Jinkwang Hwang, and Prof. Rika Hagiwara for the viscosity and Raman spectroscopy measurements.

Conflict of Interests

The authors declare that they have no known competing financial interests that could have appeared to influence the work reported in this paper.

Data Availability Statement

The data that support the findings of this study are available from the corresponding author upon reasonable request.

Keywords: lithium-ion battery · polysiloxane · room temperature performance · solid polymer electrolyte

[1] S. Randau, D. A. Weber, O. Kötz, R. Koerver, P. Braun, A. Weber, E. Ivers-Tiffée, T. Adermann, J. Kulisch, W. G. Zeier, F. H. Richter, J. Janek, *Nat. Energy* **2020**, *5*, 259–270.
[2] H. Y. Huo, J. Gao, N. Zhao, D. X. Zhang, N. G. Holmes, X. N. Li, Y. P. Sun, J. M. Fu, R. Y. Li, X. X. Guo, X. L. Sun, *Nat. Commun.* **2021**, *12*, 176.
[3] J. Kalhoff, G. G. Eshetu, D. Bresser, S. Passerini, *ChemSusChem* **2015**, *83*, 2154–75.
[4] A. Varzi, R. Raccichini, S. Passerini, B. Scrosati, *J. Mater. Chem. A* **2016**, *4*, 17251–17259.
[5] Y. Chen, Y. Shi, Y. Liang, H. Dong, F. Hao, A. Wang, Y. Zhu, X. Cui, Y. Yao, *ACS Appl. Energ. Mater.* **2019**, *2*, 1608–1615.
[6] A. D. Jenkins, P. Kratochvíl, R. F. T. Stepto, U. W. Suter, *Pure Appl. Chem.* **1996**, *68*, 2287–2311.
[7] J. B. Goodenough, Y. Kim, *Chem. Mater.* **2010**, *22*, 587–603.
[8] Y. Zheng, Y. Yao, J. Ou, M. Li, D. Luo, H. Dou, Z. Li, K. Amine, A. Yu, Z. Chen, *Chem. Soc. Rev.* **2020**, *49*, 8790–8839.
[9] G. Chen, F. Zhang, Z. Zhou, J. Li, Y. Tang, *Adv. Energy Mater.* **2018**, *8*, 1801219.
[10] C. Gao, X. Li, G. Wei, S. Wang, X. Zhao, F. Kong, *Compos. Commun.* **2022**, *33*, 101226.
[11] H. Wang, S. Chen, Y. Li, Y. Liu, Q. Jing, X. Liu, Z. Liu, X. Zhang, *Adv. Energy Mater.* **2021**, *11*, 2101057.
[12] A. Celik Kucuk, Chapter 22, *Applications of POSS nanocomposites in the energy field in Polyhedral Oligomeric Silsesquioxane (POSS) Polymer Nanocomposites* (Eds.: S. Thomas, L. Somasekharan), Elsevier, **2021**, p. 471–480.
[13] A. C. Kucuk, *J. Struct. Chem.* **2018**, *59*, 1744–1752.
[14] S. Zhao, Y. Zhang, H. Pham, J.-M. Y. Carrillo, B. G. Sumpter, J. Nanda, N. J. Dudney, T. Saito, A. P. Sokolov, P.-F. Cao, *ACS Appl. Energ. Mater.* **2020**, *3*, 12540–12548.
[15] H. Nakahara, S.-Y. Yoon, T. Piao, F. Mansfeld, S. Nutt, *J. Power Sources* **2006**, *158*, 591–599.
[16] J. Zhang, Y. Zhong, S. Wang, D. Han, M. Xiao, L. Sun, Y. Meng, *ACS Appl. Energ. Mater.* **2021**, *4*, 862–869.
[17] A. Celik-Kucuk, T. Abe, *ChemPhysChem* **2023**, *24*, e202200527.
[18] A. Celik-Kucuk, T. Abe, *J. Power Sources* **2023**, *556*, 232520.
[19] A. C. Kucuk, J. Matsui, T. Miyashita, *J. Mater. Chem. A* **2012**, *22*, 3853–3858.
[20] A. Celik Kucuk, T. Yamanaka, T. Abe, *J. Mater. Chem. A* **2020**, *8*, 22134–22142.
[21] A. C. Kucuk, J. Matsui, T. Miyashita, *J. Colloid Interface Sci.* **2011**, *355*, 106–114.
[22] A. C. Kucuk, J. Matsui, T. Miyashita, *Langmuir* **2011**, *27*, 6381–6388.
[23] A. C. Kucuk, J. Matsui, T. Miyashita, *RSC Adv.* **2018**, *8*, 2148–2156.
[24] A. C. Kucuk, J. Matsui, T. Miyashita, *Turk. J. Chem.* **2020**, *44*, 296–308.
[25] A. Celik Kucuk, O. A. Urucu, *React. Funct. Polym.* **2019**, *140*, 22–30.
[26] H. Li, Y.-M. Chen, X.-T. Ma, J.-L. Shi, B.-K. Zhu, L.-P. Zhu, *J. Membr. Sci.* **2011**, *379*, 397–402.
[27] S. M. Seidel, S. Jeschke, P. Vettikuzha, H. D. Wiemhöfer, *Chem. Commun.* **2015**, *51*, 12048–12051.
[28] H.-P. Liang, M. Zarrabeitia, Z. Chen, S. Jovanovic, S. Merz, J. Granwehr, S. Passerini, D. Bresser, *Adv. Energy Mater.* **2022**, *12*, 2200013.
[29] D. Wang, B. Jin, S. Chen, Y. Ren, Y. Hou, X. Gao, Q. He, X. Zhan, Q. Zhang, *J. Power Sources* **2023**, *564*, 232847.
[30] M. Walkowiak, G. Schroeder, B. Gierczyk, D. Waszak, M. Osińska, *Electrochem. Commun.* **2007**, *9*, 1558–1562.
[31] M. Benz, W. B. Euler, *J. Appl. Polym. Sci.* **2003**, *89*, 1093–1100.
[32] J. Evans, C. A. Vincent, P. G. Bruce, *Polymer* **1987**, *28*, 2324–2328.
[33] M. C. Borghini, M. Mastragostino, S. Passerini, B. Scrosati, *J. Electrochem. Soc.* **1995**, *142*, 2118.
[34] S. K. Shalu, Chaurasia, R. K. Singh, S. Chandra, *J. Phys. Chem. B* **2013**, *117*, 897–906.
[35] H. Kim, Y. Tian, G. Ceder, *J. Electrochem. Soc.* **2020**, *167*, 110555.
[36] M. Liu, D. Zhou, Y.-B. He, Y. Fu, X. Qin, C. Miao, H. Du, B. Li, Q.-H. Yang, Z. Lin, T. S. Zhao, F. Kang, *Nano Energy* **2016**, *22*, 278–289.
[37] Y. Xu, K. Wang, Y. An, W. Liu, C. Li, S. Zheng, X. Zhang, L. Wang, X. Sun, Y. Ma, *J. Phys. Chem. Lett.* **2021**, *12*, 10603–10609.
[38] Z. Li, J. Fu, X. Zhou, S. Gui, L. Wei, H. Yang, H. Li, X. Guo, *Adv. Sci.* **2023**, *10*, 2201718.
[39] M. Xie, S. Li, Y. Huang, Z. Wang, Y. Jiang, M. Wang, F. Wu, R. Chen, *ChemElectroChem* **2019**, *6*, 2423–2429.
[40] N. Zhang, J. He, W. Han, Y. Wang, *J. Mater. Sci.* **2019**, *54*, 9603–9612.
[41] A. Celik-Kucuk, T. Abe, *J. Power Sources* **2021**, *496*, 229828.
[42] Z. Song, X. Wang, H. Wu, W. Feng, J. Nie, H. Yu, X. Huang, M. Armand, H. Zhang, Z. Zhou, *J. Power Sources Adv.* **2022**, *14*, 100088.

Manuscript received: May 1, 2023
Revised manuscript received: June 12, 2023
Version of record online: June 21, 2023